Electronic Supplementary Material (ESI) for Journal of Materials Chemistry A.

Effect of solvent on the crystal phase, morphology, and sodium storage performance of $FeSe_2$

Manman Ren [a*#], Haoting Zang [a#], Shilei Cao [a], Hongling Guo [a], Jihui Zhang [a], Weiliang Liu [a], Jinshui Yao [a], Xu Zhang [b*], Zhen Zhou [b]

[a] School of Materials Science and Engineering, Qilu University of Technology (Shandong Academy of Sciences), Jinan 250353, PR China

[b] Interdisciplinary Research Center for Sustainable Energy Science and Engineering (IRC4SE^2), School of Chemical Engineering, Zhengzhou University, Zhengzhou 450001, P. R. China.

Materials characterization

XRD pattern was conducted on SHMADZUXRD-6100AS with Cu Kα X-ray radiation (λ=0.15406 nm). The chemical composition of the $FeSe_2$ (ESCALAB 250 X-ray spectrometer with Al Kα X-ray source) was analyzed by X-ray photoelectron spectroscopy (XPS). The morphology and microstructure details of the samples was investigated by Scanning electron microscopy (SEM, ZEISS SUPRATM 55) and transmission electron microscopy (TEM, FEI-TECNAI-G20). Raman spectra was characterized by LabRam HR confocal laser microRaman spectrometer. Brunauer-Emmet-Teller (BET) surface areas were characterized by nitrogen adsorption with Autosorb-iQ specific surface area instrument.

Electrochemical measurements

Test electrodes were composed of $FeSe_2$ (80%), acetylene black (10%), and polyvinylidene fluoride (10%). Sodium metal and microporous glass fiber were used as

the counter electrodes and separator. The electrolyte was 1.0 M $NaSO_3CF_3$ dissolved in the diglyme. Galvanostatic charge/discharge tests of 0.3-3.0 V (vs. Na^+/Na) were carried out on the Neware battery testing system. The cyclic voltammetry (CV) and electrochemical impedance spectroscopy (EIS) were studied by CHI760 E electrochemical workstation. The CV curves at different scan rates were tested in the potential range of 0.3-3.0 V (vs. Na^+/Na). EIS was studied in the frequency range of 100 -0.01 Hz with an amplitude of 5 mV. The galvanostatic discharge/charge tests and GITT were conducted on NEWARE battery test systems, with a potential range of 0.3~3.0 V (vs. Na^+/Na).

Computational methods

The spin-polarized density functional theory (DFT) calculations were performed using Vienna ab initio simulation package (VASP) with the plane-wave techniques.[1] The Perdew-Burke-Ernzerhof (PBE) functional within the generalized gradient approximation (GGA) was adopted to describe the exchange-correlation interaction.[2] A kinetic cutoff energy of 450 eV was used for the plane-wave basis set. In order to accurately deal with the long-rang van der Waals (vdW) interactions, the zero damping DFT-D3 method of Grimme was used.[3] A vacuum layer of 20 Å was inserted to eliminate the artificial interactions between the periodically repeated layers. A Monkhorst-Pach scheme with a *K*-point mesh of 0.03 1/Å density was used in the computations.[4] According to our experiments, $FeSe_2$, (101) and (110) surfaces were built. For the computations of $FeSe_2$ surfaces, the lower one-third atoms were fixed and other atoms were fully relaxed. The adsorption energy (E_{ads}) of Na atom on the $FeSe_2$

surface was calculated from the equation:

$$E_{ads} = E_{Na\text{-}surface} - E_{surface} - E_{Na}$$

in which $E_{Na\text{-}surface}$ is the total energy of Na atom adsorbed on the $FeSe_2$ surface and $E_{surface}$ and E_{Na} are the energy of $FeSe_2$ surface and Na atom in Na metal bulk, respectively. The Na migration pathways on the $FeSe_2$ surfaces and corresponding energy barriers were calculated based on the climbing-image nudged elastic band (CI-NEB) method.[5]

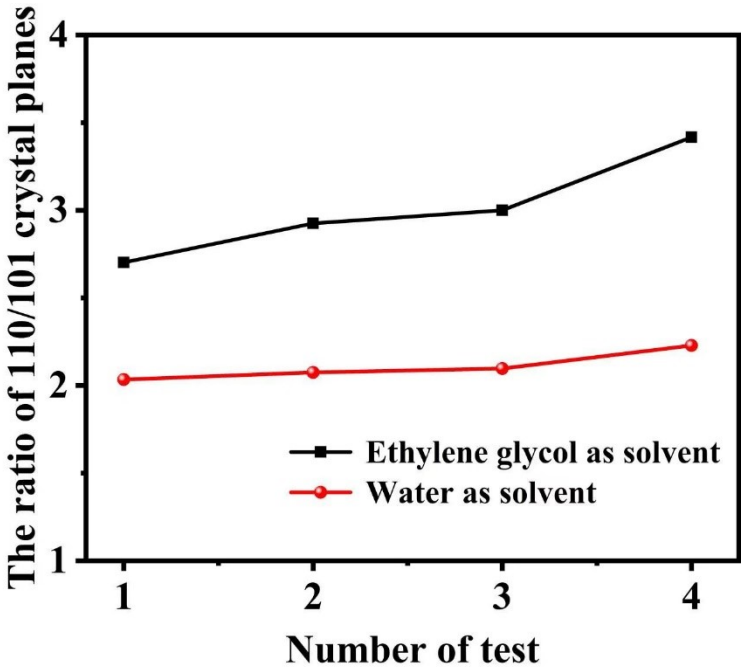

Fig. S1 The ratio of 110/101 crystal planes in $FeSe_2$/rGO-EG

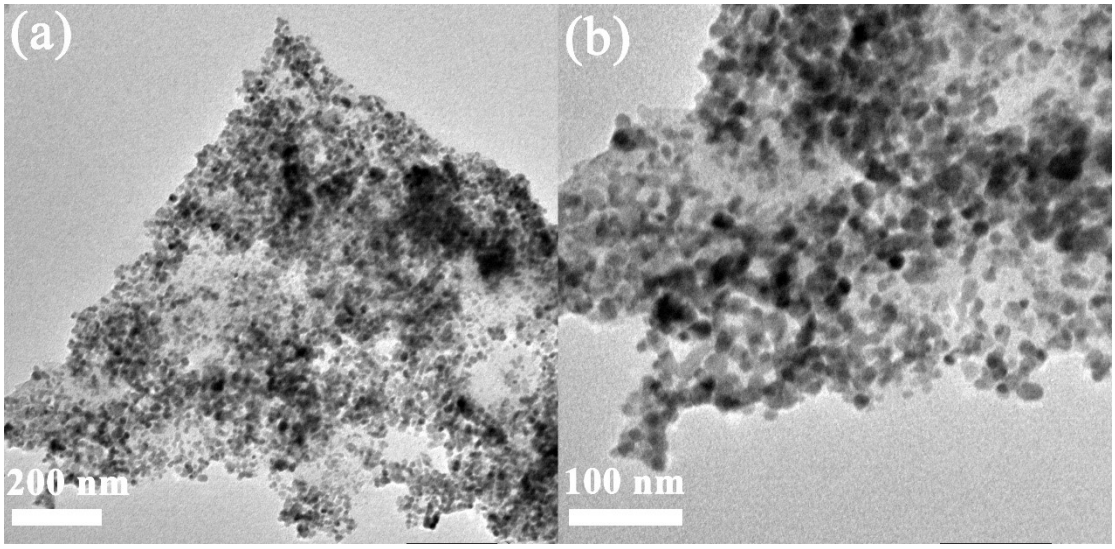

Fig. S2 TEM images of Fe_3O_4/rGO

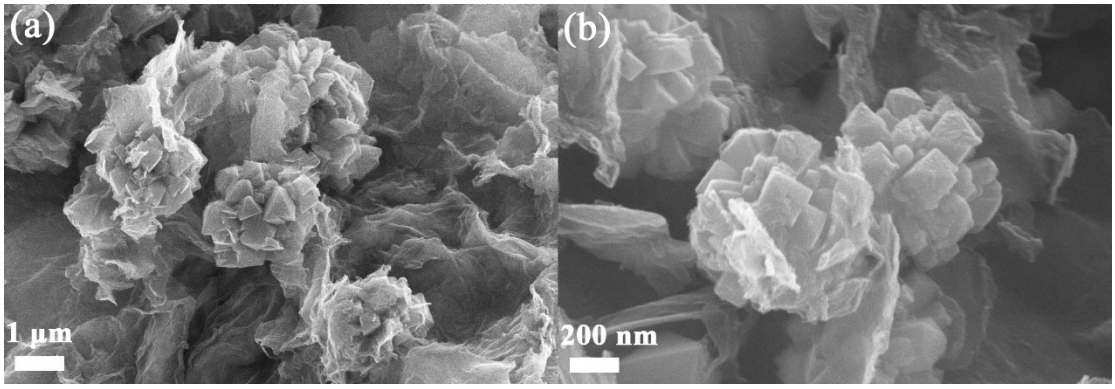

Fig. S3 SEM images of $FeSe_2$/rGO-EG at different solvothermal reaction time (a) 5h and (b) 15h

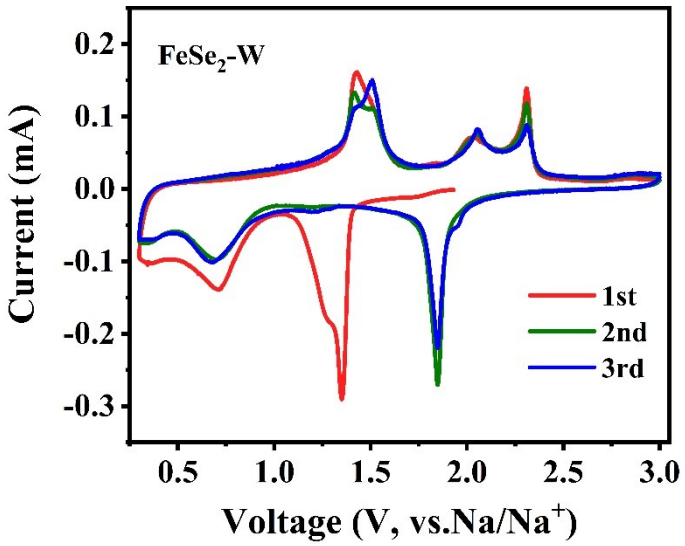

Fig. S4 CV profiles of the $FeSe_2$/rGO-W electrode at 0.1 mV s^{-1}

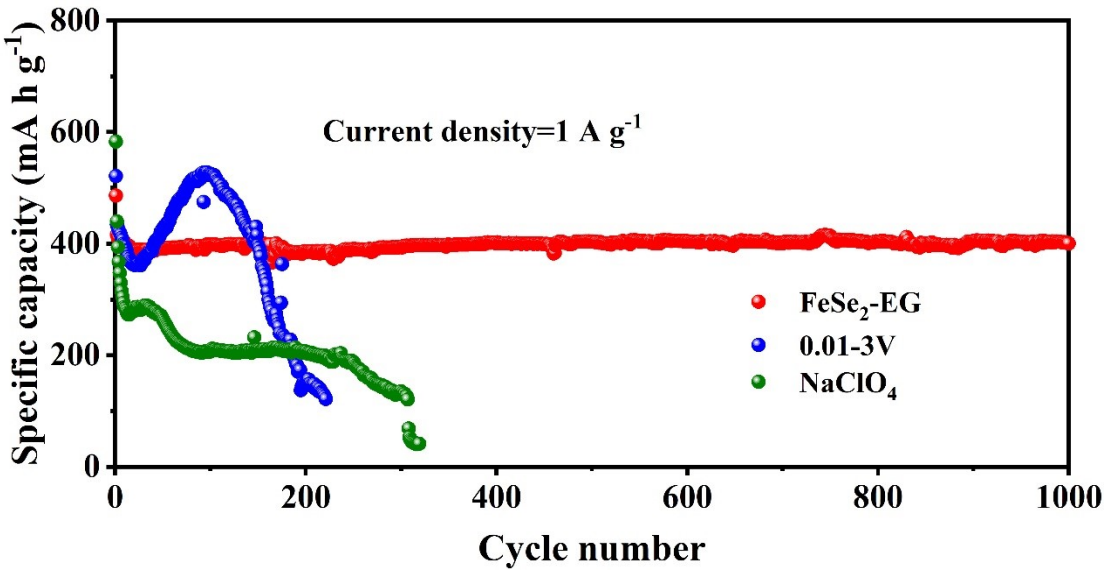

Fig. S5 Long cycling performance of the $FeSe_2$/rGO-EG electrode at 1 A g^{-1} under different situations.

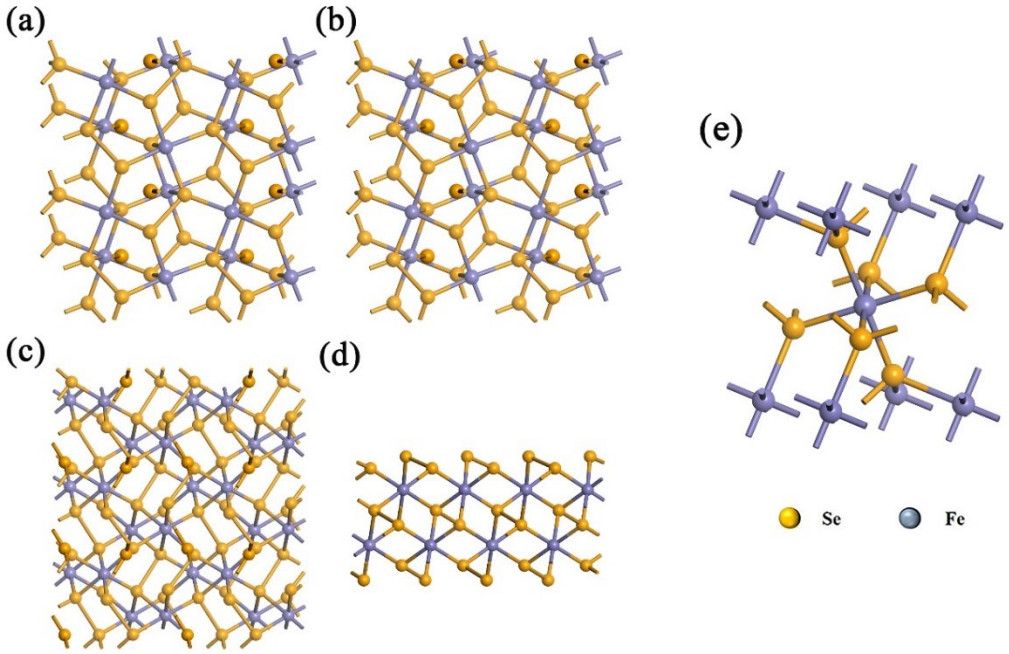

Fig. S6 (a, b) Optimized atomic configuration of top and side view of (110) plane; (c,d) Optimized atomic configuration of top and side view of (101) plane; (e) Optimized atomic cofiguration of $FeSe_2$.

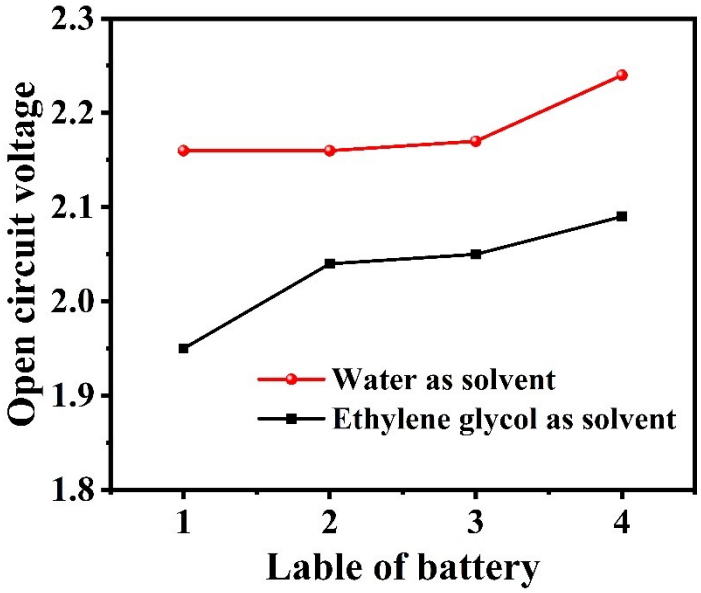

Fig. S7 Open circuit voltage of the $FeSe_2$/rGO-EG and $FeSe_2$/rGO-W electrodes

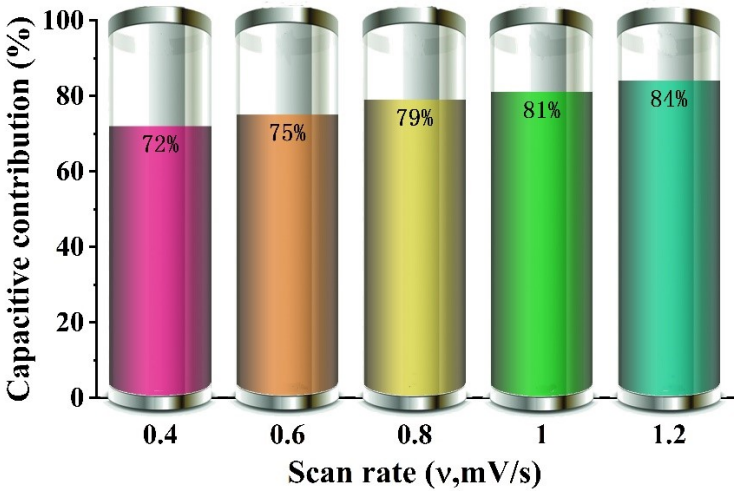

Fig. S8 Capacitive contribution to the total capacity of the $FeSe_2$/rGO-W electrodes at various scan rates

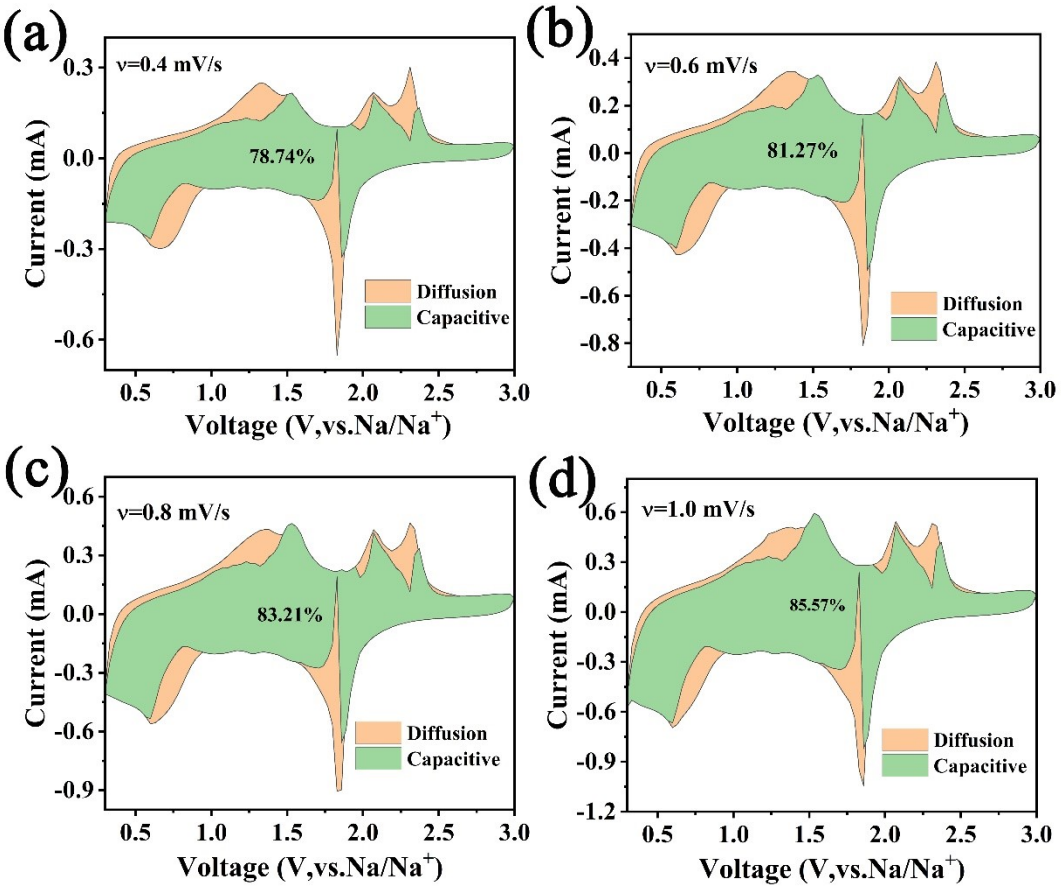

Fig. S9 Diffusion-controlled and capacitive contribution of the $FeSe_2$/rGO-EG electrodes at 0.4 mV s^{-1} (a), 0.6 mV s^{-1} (b), 0.8 mV s^{-1} (c), 1.0 mV s^{-1} (d).

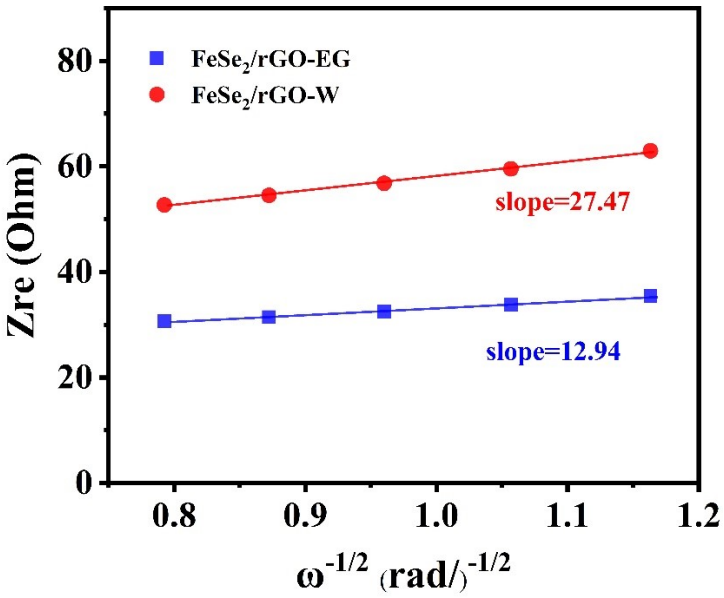

Fig. S10 Linear fits in low-frequency regions of the $FeSe_2$/rGO-EG and $FeSe_2$/rGO-W

Table S1 Comparison of the electrochemical performances of the $FeSe_2$/rGO-EG and other $FeSe_2$-based anode material.

Samples	Current density (A /g)	Cycle number (n)	Capacity (mAh /g)	Solvent	Ref
$FeSe_2$@C	1.0	200	359	H_2O / isopropyl alcohol	[6]
O-$FeSe_2$ NSs	1.0	700	268	Oleylamine	[7]
$FeSe_2$@C/NG	0.5	160	350	H_2O	[8]
$FeSe_2$@GC-rGO	1.0	150	393	DMF	[9]
$FeSe_2$-HGCNS	0.5	100	425	DMF	[10]
$FeSe_2$ NPs/CB	0.8	300	450	Oleylamine /1-octadecene	[11]
FCSe@C@void@C	0.4	400	282	H_2O	[12]
$FeSe_x$-rGO	1.0	1000	311	H_2O	[13]
$FeSe_2$/rGO-EG	1.0	1000	400	Ethylene glycol	This work

References:

1. G. Kresse and J. Furthmüller, *Phys Rev B*, 1996, **54**, 11169-11186.
2. J. P. Perdew, K. Burke and M. Ernzerhof, *Phys Rev Lett*, 1996, **77**, 3865-3868.
3. S. Grimme, J. Antony, S. Ehrlich and H. Krieg, *J Chem Phys*, 2010, **132**, 154104.
4. H. J. Monkhorst and J. D. Pack, *Phys Rev B*, 1976, **13**, 5188-5192.
5. G. Henkelman and H. Jónsson, *J Chem Phys*, 2000, **113**, 9978-9985.
6. T. Wang, W. Guo, G. Wang, H. Wang, J. Bai and B. Wang, *Journal of Alloys and Compounds*, 2020, **834**. 155265
7. Z.-Q. Wang, B. Zeng, D. Zhou, L. Tai, X.-D. Liu and W.-M. Lau, *Chemical Engineering Journal*, 2022, **428**. 132637
8. S. H. Yang, S. K. Park and Y. C. Kang, *International Journal of Energy Research*, 2021, **45**, 20909-20920.
9. J. S. Cho, J. K. Lee and Y. C. Kang, *Sci Rep*, 2016, **6**, 23699.
10. J.-S. Park, S. Y. Jeong, K. M. Jeon, Y. C. Kang and J. S. Cho, *Chemical Engineering Journal*, 2018, **339**, 97-107.
11. F. Zhao, S. Shen, L. Cheng, L. Ma, J. Zhou, H. Ye, N. Han, T. Wu, Y. Li and J. Lu, *Nano Lett*, 2017, **17**, 4137-4142.
12. J. Wang, B. Wang, H. Sun, G. Wang, J. Bai and H. Wang, *Energy Storage Materials*, 2022, **46**, 394-405.
13. G. D. Park, J. S. Cho, J. K. Lee and Y. C. Kang, *Sci Rep*, 2016, **6**, 22432.